atmosphere

Article

Convection-Permitting Regional Climate Simulation over Bulgaria: Assessment of Precipitation Statistics

Rilka Valcheva *, Ivan Popov and Nikola Gerganov

National Institute of Meteorology and Hydrology, 1784 Sofia, Bulgaria; ivan.popov@meteo.bg (I.P.)
* Correspondence: rilka.valcheva@gmail.com

Abstract: With increasing computational power, the regional climate modeling community is moving to higher resolutions of a few kilometers, named convection-permitting (CP) simulations. This study aims to present an assessment of precipitation metrics simulated with the non-hydrostatic regional climate model RegCM-4.7.1 at CP scale for a decade-long period (2001–2010) for Bulgaria. The regional climate simulation at 15 km grid spacing uses ERA-Interim ($0.75^{\circ} \times 0.75^{\circ}$) re-analysis as the driving data and parametrized deep convection. The kilometer-scale simulation at 3 km horizontal grid spacing is nested into regional climate simulation using parametrized shallow convection only. The CP simulation is evaluated against daily and hourly datasets available for the selected period and is compared with the coarser resolution driving simulation. The results show that the model represents well the spatial distribution of mean precipitation at the regional and kilometer scale for the territory of Bulgaria. However, the CP_RegCM_3km model produces too much precipitation over the mountains and shows the largest biases in the summer season (above 100%). At the daily scale, improvements are found in CP simulation for precipitation wet-day intensity and extreme precipitation in the autumn and for wet-day frequency in the summer. At the hourly scale, the kilometer-scale simulation improved the performance of wet-hour precipitation intensity in all seasons compared with coarse-resolution simulation (−23% vs. −46% in MAM; −10% vs. −37% in JJA; −47% vs. −53% in SON; −54% vs. −62% in DJF) and extreme precipitation in the autumn (−7% vs. −51%) and winter (−34% vs. −58%). The representation of wet-hour frequency was improved by CP_RegCM_3km in all seasons, except summer (−3.1% vs. −6.7% in spring; 0.5% vs. −3.8% in autumn and −7.7% vs. −11.5% in winter).

Keywords: non-hydrostatic RegCM4; convection-permitting modeling; extreme precipitation; frequency; intensity; regional climate modeling; Bulgaria; kilometer scale

check for updates

Citation: Valcheva, R.; Popov, I.; Gerganov, N. Convection-Permitting Regional Climate Simulation over Bulgaria: Assessment of Precipitation Statistics. *Atmosphere* **2023**, *14*, 1249. https://doi.org/10.3390/atmos14081249

Academic Editors: Kostadin Ganev and Georgi Gadzhev

Received: 12 July 2023
Revised: 31 July 2023
Accepted: 3 August 2023
Published: 5 August 2023

Copyright: © 2023 by the authors. Licensee MDPI, Basel, Switzerland. This article is an open access article distributed under the terms and conditions of the Creative Commons Attribution (CC BY) license (https://creativecommons.org/licenses/by/4.0/).

1. Introduction

About a decade ago, the development of high-performance computing systems and regional climate models (RCMs) allowed long-term, very high-resolution (1–4 km) simulations, called "convection-permitting" (CP) simulations [1–4]. The convection-permitting regional climate models (CP-RCMs) allow the explicit representation of deep convective processes without the use of parametrization schemes, which is considered to be a major source of model errors and uncertainty with regard to rainfall and related precipitation [1,5–7].

The regional climate model version 4 (RegCM4) developed at the Abdus Salam International Centre for Theoretical Physics ICTP [3,8] has been recently upgraded with the non-hydrostatic dynamic core based on MM5, which can be used for high-resolution applications [3]. The non-hydrostatic RegCM contributes to several large projects at the kilometer scale, such as the European Climate Prediction system (EUCP) [9], the Coordinated Regional Climate Downscaling Experiment Flagship Pilot Studies on convective phenomena (CORDEX-FPS) [2], and it is used by a large modeling community.

Recent studies using decade-long CP regional climate simulations show that increasing the grid spacing reduces the present-day biases in precipitation [10,11]. The results confirm the improved performance of convection-permitting models compared with coarser resolution models in simulating important characteristics of daily and hourly precipitation and extreme events [11]. Pichelli [12] shows the first multi-model future simulations over the Alps. The simulations show increases in future high-impact events' frequency and intensity of the summer and autumn precipitation. Similar studies highlighting the beneficial impact of removing any parameterization of convection processes are described in Capecchi [13], Giordani [14], Adinolfi [15], and Fosser [16]. Motivated by these results, we use the non-hydrostatic RegCM4 model for the territory of Bulgaria. The performance of the RegCM4 model in capturing different precipitation statistics for Bulgaria has not been extensively investigated [17,18]. The innovative aspect of the study is that, as far as we know, no previous study exists with regard to convection-permitting climate simulations for the Bulgarian domain.

The aim of this study is to present an initial assessment of precipitation simulated with the non-hydrostatic regional climate model RegCM (version 4.7.1, released in 2019) at a regional and convection-permitting (CP) scale for a decade-long period (2001–2010) for Bulgaria. The period was chosen following the CORDEX-FPS protocol [2].

The structure of the manuscript is as follows: Section 2 presents the model, data, and methodology of this study; Section 3 presents the results of the assessment of precipitation mean, intensity, frequency, and extreme precipitation; and Section 4 provides a discussion and conclusion.

2. Model, Data, and Methods

Bulgaria (see Figure 1) is located in southeastern Europe and exhibits a wide range of climatic conditions due to its geographical position between the Mediterranean and continental climatic regimes. The country's terrain is characterized by mountains, valleys, and coastal areas, presenting a challenging environment for climate models to accurately simulate local-scale weather phenomena and associated precipitation patterns. Proper representation of precipitation is of primary importance for various sectors, including agriculture, water resources management, and disaster preparedness, making it crucial to evaluate the capability of climate models to reproduce precipitation characteristics for Bulgaria in the present and future.

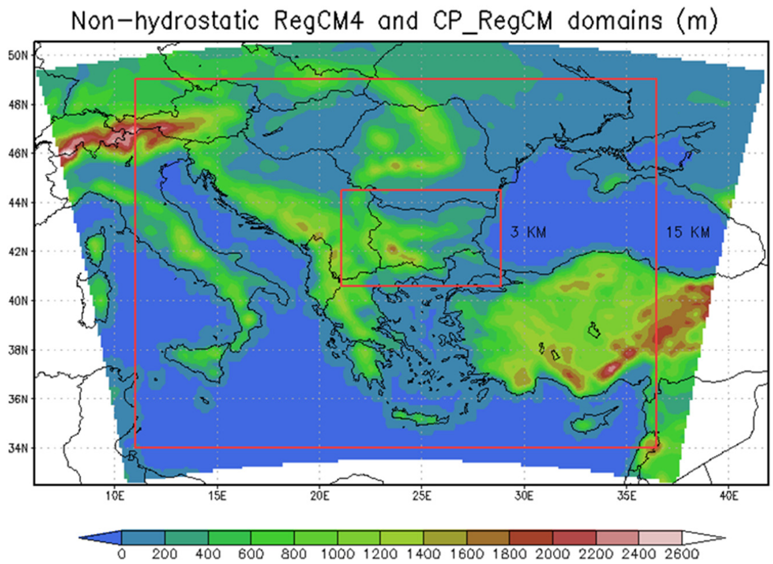

Figure 1. Domains simulated with non-hydrostatic RegCM4.7.1 at regional and CP scales: intermediate domain with 15 km grid size (RegCM_15km) (6.08° E–41.96° E, 32.47° N–50.54° N) and nested domain with 3 km grid size (CP_RegCM_3km) (19.91° E–30.09° E, 39.76° N–45.32° N) after removing the buffer zone (red lines) from 15 and 30 grid points from each side, respectively. The orography is shown in (m).

The CP simulation (780 km × 600 km) with a horizontal grid spacing of 3 km (CP_RegCM_3km) is nested into regional climate simulation at 15 km grid spacing (RegCM_15km) driven by the ERA-Interim [19] re-analysis (0.75° × 0.75°) (Figure 1). RegCM_15km simulation uses parametrized deep convection, while CP_RegCM_3km uses parametrized shallow convection only. The kilometer-scale simulation is evaluated against the daily (MESCAN-SURFEX (5.5 km × 5.5 km), E-OBS v25.e (0.1° × 0.1°), CHIRPS (0.05° × 0.05°)) and hourly (PERSIAN PDIR-Now (0.04° × 0.04°)) datasets available for the period 2001–2010 and is compared with the coarser resolution driving simulation. For both simulations, CP and regional scale, we use the year 2000 as a spin-up, and this year is removed from the analysis. We focus on different precipitation statistics, such as seasonal mean daily precipitation, seasonal wet-day and -hour intensity, seasonal wet-day and -hour frequency, and seasonal extreme precipitation (99th percentile of all daily and 99.9th percentile of all hourly precipitation events). The simulations are carried out on the Bulgarian European High Performance Computing Joint Undertaking (EuroHPC JU) supercomputer Discoverer, located in Sofia Tech Park in Sofia, Bulgaria (https://sofiatech.bg/en/petascale-supercomputer/, accessed on 15 April 2022). Using 4 nodes and 128 computing cores of the Discoverer supercomputer, 1-month simulation is performed in approximately 5.6 h.

In this study, both 10-year simulations (RegCM_15km and CP_RegCM_3km) use the newly developed non-hydrostatic dynamic core [3] of the RegCM4 [8] model, CCSM radiation [20], modified Holtslag planetary boundary scheme [21], SUBEX microphysics scheme [22], land surface scheme BATS [23], and Zeng ocean fluxes scheme [24]. For the intermediate simulation, we use the Kain–Fritsch cumulus convection scheme [25,26]. For the convection-permitting (CP) simulations, we use the MM5 shallow cumulus scheme [3,27]. This configuration was chosen in a previous study [28], showing the best results for the studied territory. The ERA-Interim re-analysis [19] is used to provide the initial and lateral boundary conditions for the intermediate run at 15 km grid spacing updated every 6 h covering the Balkan Peninsula region, which, on the other hand, provides the initial and lateral boundary conditions for the convection-permitting run at 3 km grid spacing.

To assess the model's ability to produce precipitation climatology, several statistical indices are used (defined in Table 1). The indices are calculated as seasonal values for all seasons: spring (March–April–May, MAM), summer (June–July–August, JJA), autumn (September–October–November, SON), and winter (December–January–February, DJF). The observational datasets are remapped using the distance weighted interpolation method onto a 3 km grid for the evaluation of the kilometer-scale CP_RegCM_3km simulation and onto a 15 km grid for the evaluation of the RegCM_15km simulation.

Table 1. Statistical indices for daily and hourly precipitation used in this study.

Statistical Indices	Definition	Units
Mean precipitation	Daily mean precipitation.	mm/day
Frequency	Wet-day/hour frequency, defined as a percentage of the number of wet days/hours per season; wet day/hour is a day/hour with precipitation ≥ 1 mm/0.1 mm.	(%)
Intensity	Wet-day/hour intensity, defined as a day/hour with precipitation ≥1 mm/0.1 mm.	mm/day; mm/hour
Heavy precipitation (p99/p99.9)	P99 and P99.9 percentiles, defined as the 99th/99.9th percentile of all daily/hourly precipitation events; percentiles are calculated using all events (wet and dry) following Schär [29].	mm/day; mm/hour
Mean bias	RegCM—Observation.	mm/day; mm/hour and (%)

To analyze the spatial properties of precipitation in the models (CP_RegCM_3km and RegCM_15km), we use the following precipitation indices: mean daily precipitation amount, mean wet-day/hour precipitation intensity, wet-day/hour frequency, 99th percentiles of all daily (wet and dry) precipitation events, and 99.9th percentiles of all hourly (wet and dry) precipitation events. A wet day is defined as a day with precipitation larger than or equal to 1 mm/day, while a wet hour is defined as an hour with precipitation larger than or equal to 0.1 mm/hour (see Table 1).

A key issue when validating kilometer-scale simulation is the availability of high-resolution and quality datasets. Precipitation measurements come from different sources, such as in situ rain gauges, radars, and satellites. In our study, we use four different observational datasets based on different sources available for the study period 2001–2010 (Table 2) to assess daily and hourly precipitation: E-OBS v.25e—station-based observational ensemble mean daily precipitation data available at 0.1° grid spacing; CHIRPS—daily dataset based on stations and satellites available at 0.05° spatial resolution; UERRA—daily re-analysis from the MESCAN-SURFEX system (5.5 × 5.5 km); PERSIAN-PDIR-Now (PERSIANN Dynamic Infrared–Rain Rate)—quasi-global, infrared-based precipitation estimates available at 0.04° × 0.04° spatial resolution from satellites for assessing hourly precipitation metrics. Hereafter, we will refer to these datasets as E-OBS, CHIRPS, MESCAN, and PDIR for short.

Table 2. Different observational datasets used in this study.

Name/Availability	Spatial Resolution	Temporal Resolution	Data Source and Region	Reference
E-OBS v.25e (1950–2021)	0.1° × 0.1°	daily	Station (Europe)	[30]
CHIRPS (1981–now)	0.05° × 0.05°	daily	Station+Satellite (Global)	[31]
MESCAN-SURFEX (1961–2019)	5.5 × 5.5 km	daily	Surface Re-Analysis (Europe)	[32,33]
PERSIAN-PDIR-Now (March 2000–now)	0.04° × 0.04°	hourly	Satellite (Global)	[34]

When dealing with observations, we should consider the uncertainties associated with the different types of sensors for precipitation measurement. For in situ data, the uncertainties are mostly related to the station's density, for example, low density over mountains, the choice of interpolation technique—which can cause underestimation of high-precipitation intensities—problems with gauge under-catch in windy conditions [35], and others. Radar measurements, on the other hand, present masking-effect problems in high-latitude areas, while in the case of satellite data, the precipitation measurements can be affected by large uncertainties linked to physical limitations and the measurement techniques and algorithms used to derive precipitation from interferometry data [36–38]. This is the reason why different observational datasets can have different performances in terms of precipitation climatology and can differ significantly, especially over terrains with low data availability [35].

3. Results

3.1. Daily Precipitation Metrics

Figure 2 compares the spatial distribution of the analyzed seasonal mean precipitation indices based on observations (CHIRPS (first column), E-OBS (second column), MESCAN (third column)) and simulations (CP_RegCM_3km (fourth column) and RegCM_15km (last column)) for the MAM (Figure 2a) and JJA (Figure 2b) seasons.

In the spring (Figure 2a), CP_RegCM_3km overestimates all indices, especially over the mountains. As we can see from Figure 2, observations differ from each other, especially CHIRPS wet-day intensity. CHIRPS shows an overestimation of precipitation wet-day intensity compared with MESCAN and E-OBS datasets and an underestimation of wet-day frequency. E-OBS underestimates mean and heavy precipitation (p99) compared with CHIRPS and MESCAN. Overall, RegCM_15km and CP_RegCM_3km capture the spatial distribution of mean, intensity, frequency, and heavy precipitation (p99); however, CP_RegCM_3km overestimates all indices, especially over the topography.

In the summer (Figure 2b), CP_RegCM_3km shows a significant overestimation of heavy precipitation (p99), especially over the mountains. CHIRPS overestimates wet-day intensity and p99 compared with E-OBS and MESCAN. Compared with the MESCAN dataset, both models show a more realistic distribution of mean daily precipitation and wet-day frequency than E-OBS and CHIRPS. CHIRPS underestimates wet-day frequency and overestimates wet-day intensity and heavy precipitation (p99) compared with the E-OBS and MESCAN datasets.

Figure 3 compares the spatial distribution of the analyzed seasonal mean precipitation indices based on observations (CHIRPS (first column), E-OBS (second column), MESCAN (third column)) and simulations (CP_RegCM_3km (fourth column) and RegCM_15km (last column)) for the SON (Figure 3a) and DJF (Figure 3b) seasons.

In the autumn season (Figure 3a), the models and observations show similar spatial distribution of daily mean precipitation. However, CP_RegCM_3km overestimates precipitation over the mountains, while RegCM_15km underestimates it compared with observations. CP_RegCM3km and MESCAN show similar spatial distribution of wet-day intensity; RegCM_15km underestimates wet-day precipitation intensity compared with the three observations. CHIRPS overestimates wet-day intensity and underestimates wet-day frequency compared with E-OBS and MESCAN. Both models overestimate wet-day frequency; CP simulation overestimates heavy precipitation (p99), especially over the mountains, while RegCM_15km underestimates extreme precipitation (p99) compared with MESCAN and CHIRPS.

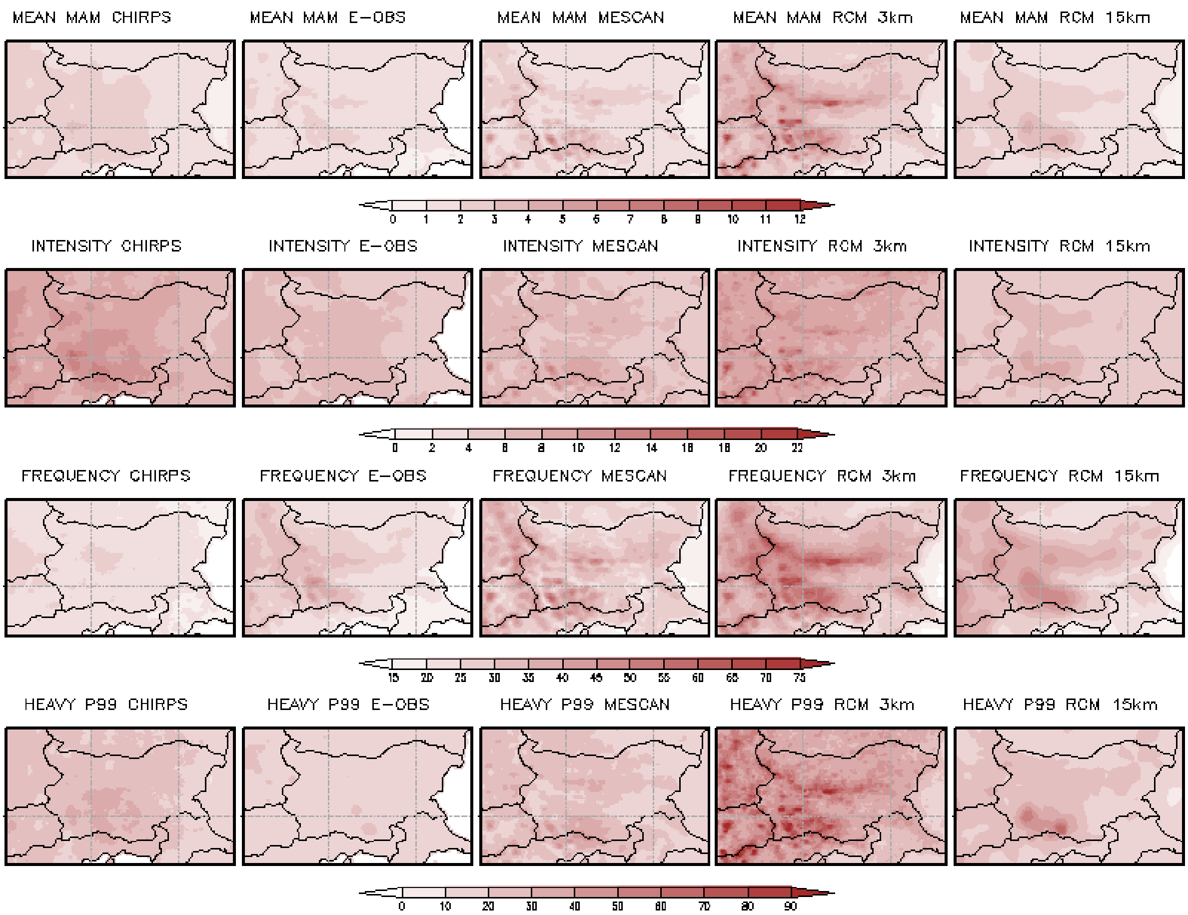

(**a**) MAM

Figure 2. *Cont.*

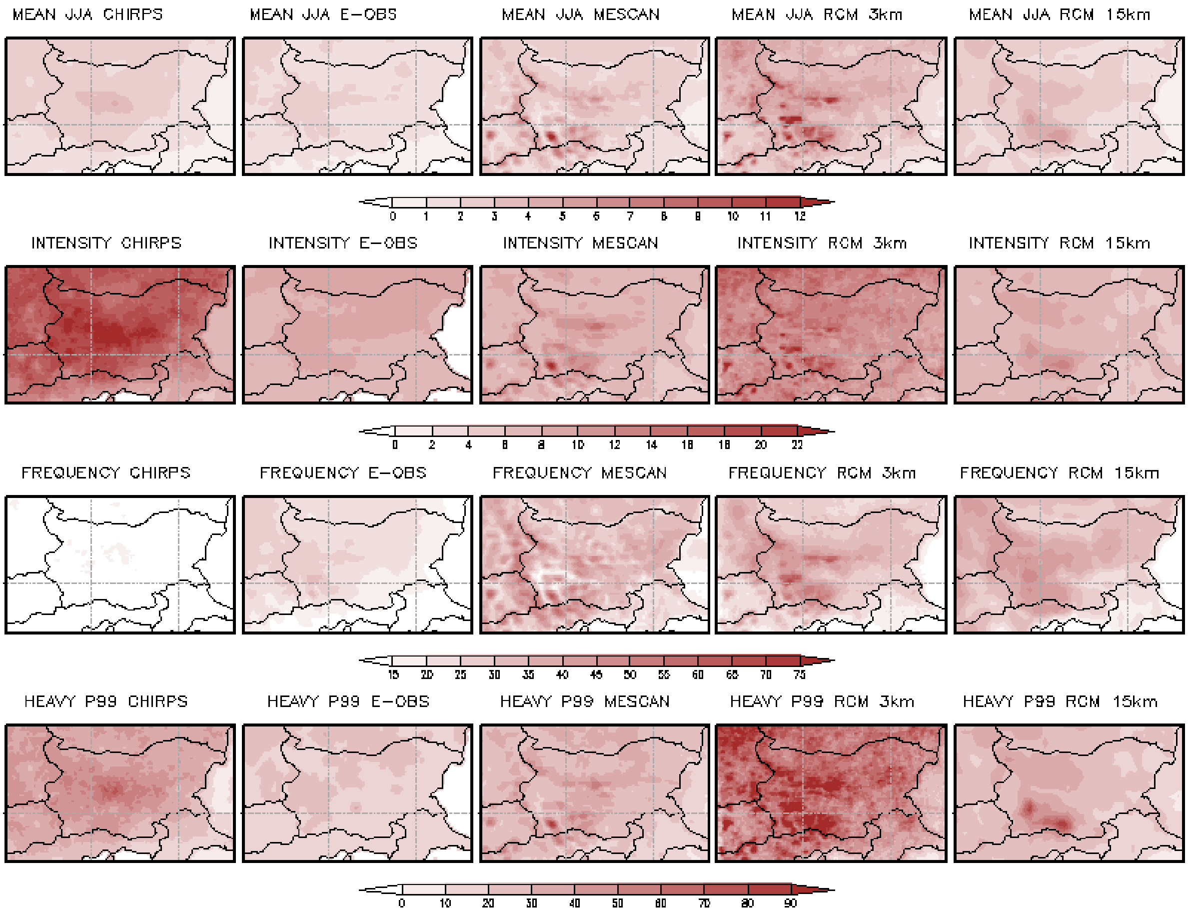

(**b**) JJA

Figure 2. Spatial distribution of analyzed indices. From top to bottom for each panel: mean daily precipitation, wet-day precipitation intensity, wet-day precipitation frequency, and heavy precipitation, defined as the 99th percentile of all daily precipitation events based on observations (CHIRPS (first column), E-OBS (second column), MESCAN-SURFEX (third column)) and simulations (CP_RegCM_3 km (fourth column) and RegCM_15 km (last column)) for the spring, MAM (**a**) and summer, JJA (**b**). The domain grid size is 19.91° E–30.09° E, 39.76° N–45.32° N.

In the winter season (Figure 3b), CP_RegCM_3km overestimates all indices over the mountains. RegCM_15km overestimates wet-day frequency over the mountains compared with the three observational datasets. CP simulation shows a similar spatial distribution of wet-day intensity compared with the CHIRPS and MESCAN datasets. In the case of heavy precipitation (p99), RegCM_15km and E-OBS overestimate it, MESCAN underestimates it, and the results are similar to the CHIRPS dataset, while kilometer-scale simulations show similar spatial distribution with MESCAN data, but MESCAN overestimates p99 over high peaks in the mountains.

The comparison among the datasets confirms that the uncertainty associated with precipitation observational data can be large, especially when dealing with precipitation intensity and extremes. The CHIRPS dataset, for example, shows a significant overestimation of wet-day precipitation intensity in JJA (Figure 2b) and SON (Figure 3a) and heavy precipitation (p99) in the summer (Figure 2b) compared with other observational datasets and also an underestimation of wet-day precipitation frequency in these seasons (Figures 2b and 3a). On the other hand, E-OBS underestimates heavy precipitation (p99) in all seasons compared with other observational datasets.

For additional information, Figures 4–6 show the spatial distribution of seasonal mean biases of daily mean precipitation (first row), wet-day precipitation intensity (second row), wet-day precipitation frequency (third row), and heavy precipitation, defined as the 99th percentile of all daily precipitation events (fourth row), between CP_RegCM_3km and E-OBS (Figure 4a), RegCM_15km and E-OBS (Figure 4b), CP_RegCM_3km and CHIRPS (Figure 5a), RegCM_15km and CHIRPS (Figure 5b), CP_RegCM_3km and MESCAN (Figure 6a), and RegCM_15km and MESCAN (Figure 6b). From left to right, the seasons are defined as spring (MAM), summer (JJA), autumn (SON), and winter (DJF) for each panel.

Compared with the E-OBS dataset (Figure 4a,b and Table 3), the biggest biases in the kilometer-scale simulation (Figure 4a) were found in JJA for wet-day intensity and heavy precipitation (p99) and over the mountains for all indices. RegCM_15km underestimates wet-day intensity in all seasons (Figure 4b), while CP_RegCM_3km overestimates intensity in MAM and JJA and over the mountains in SON and DJF. Compared with the E-OBS data, CP_RegCM_3km shows a large overestimation of extreme precipitation (p99), especially in the spring and summer (above 100%). Compared with the E-OBS data, we found improvements in kilometer-scale simulation for summer wet-day frequency (9.8% vs. 11.6%) and for autumn wet-day intensity (1.3% vs. 22%) compared with the coarse-resolution simulation (Table 3).

Compared with the CHIRPS dataset (Figure 5a,b and Table 3), we found improvements in the kilometer-scale simulation (Figure 5a) for precipitation intensity in all seasons (−1.2% vs. −35% in MAM; −24% vs. −56% in JJA; −37% vs. −52% in SON; and −8% vs. −31% in DJF) in summer wet-day frequency (16.9% vs. 18.2%) and in autumn extreme precipitation (p99) (15% vs. −35%). We found different behaviors when simulating mean precipitation in SON and DJF, where CP_RegCM_3km overestimated and RegCM_15km underestimated the daily mean precipitation. Additionally, when simulating heavy precipitation, CP_RegCM_3km overestimated heavy precipitation (p99) in all seasons, especially in the summer and spring, while RegCM_15km underestimated the p99, especially in the summer and autumn (Figure 5b). Both models overestimated wet-day frequency compared with the CHIRPS data.

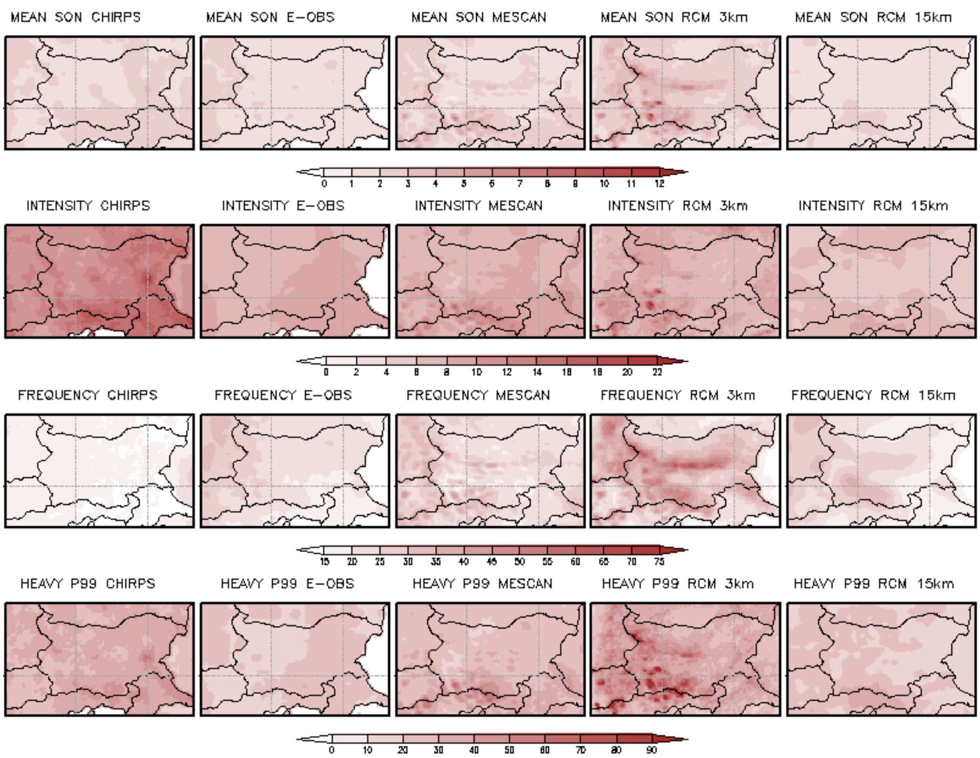

(**a**) SON

Figure 3. *Cont.*

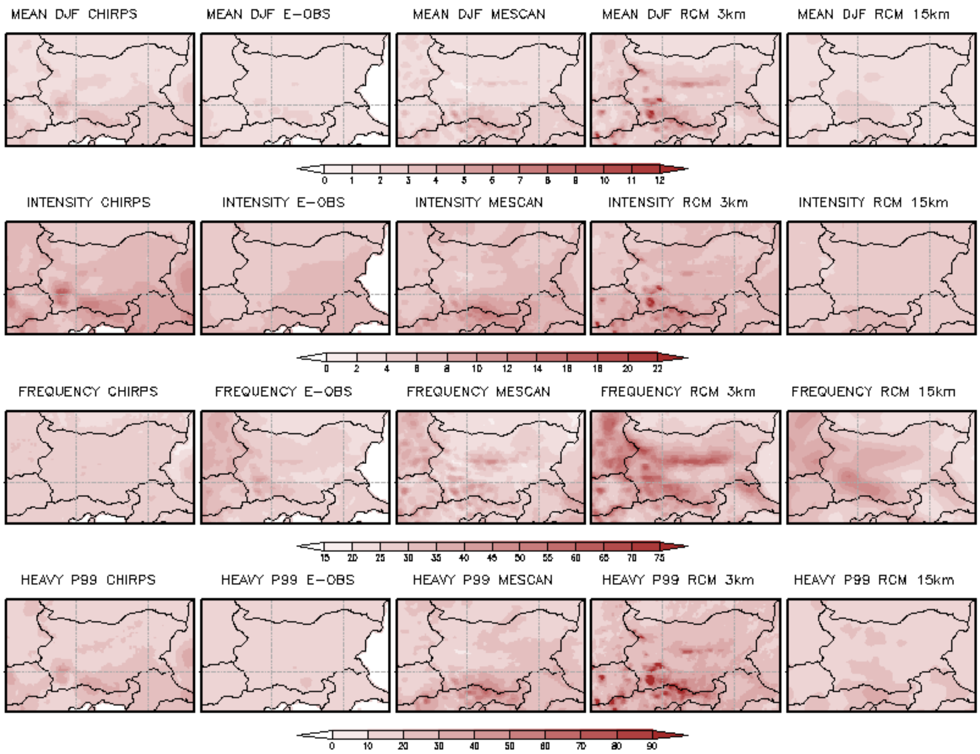

(**b**) DJF

Figure 3. Same as Figure 2, but for the (**a**) autumn (SON) and (**b**) winter (DJF) seasons. The domain grid size is 19.91° E–30.09° E, 39.76° N–45.32° N.

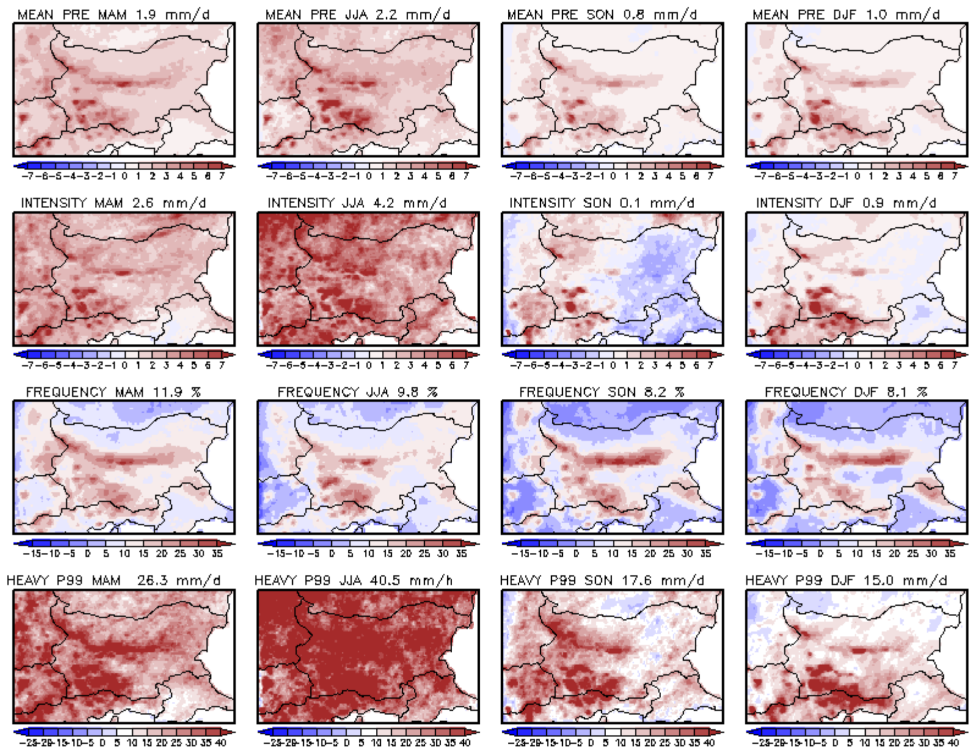

(**a**) CP_RegCM_3 km vs. E-OBS

Figure 4. *Cont.*

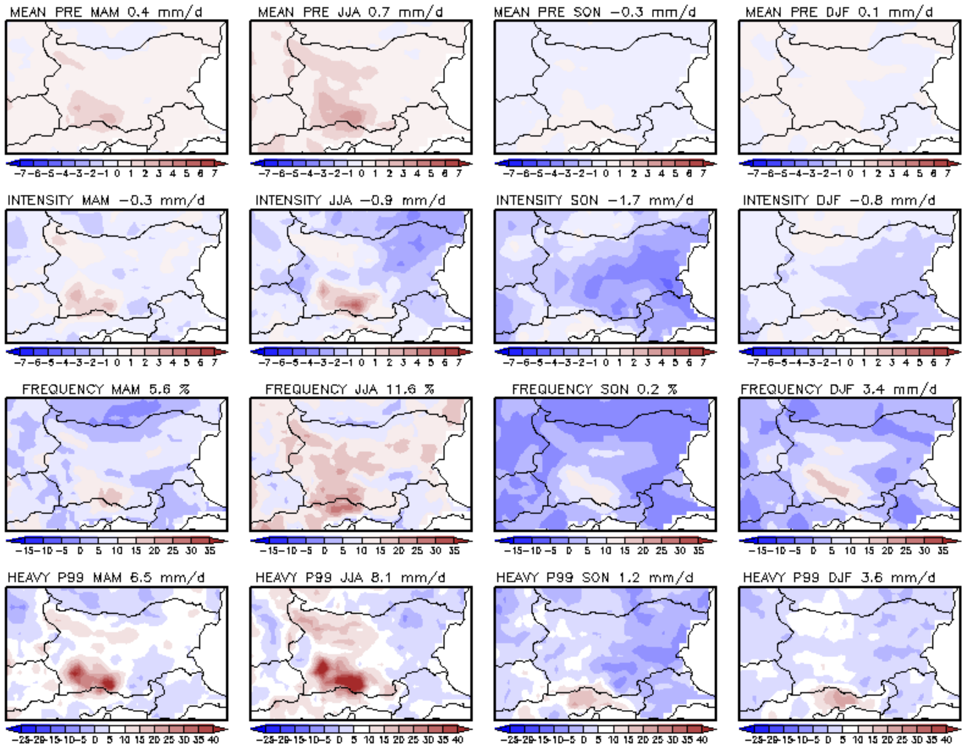

(**b**) RegCM_15 km vs. E-OBS

Figure 4. Spatial maps of seasonal mean biases of daily mean precipitation (first row), wet−day precipitation intensity (second row), wet−day precipitation frequency (third row), and heavy precipitation, defined as the 99th percentile of all daily precipitation events (fourth row), between (**a**) CP_RegCM_3 km and E-OBS; and (**b**) RegCM_15 km and E−OBS. From left to right, for each panel, the seasons are defined as spring (MAM), summer (JJA), autumn (SON), and winter (DJF). The domain grid size is 19.91° E–30.09° E, 39.76° N–45.32° N.

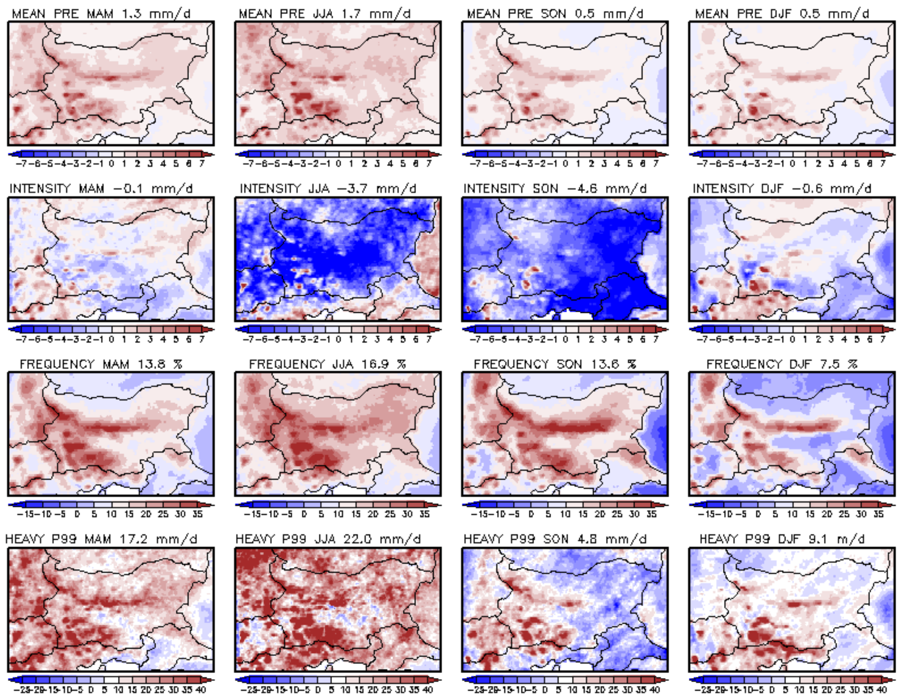

(**a**) CP_RegCM_3 km vs. CHIRPS

Figure 5. *Cont.*

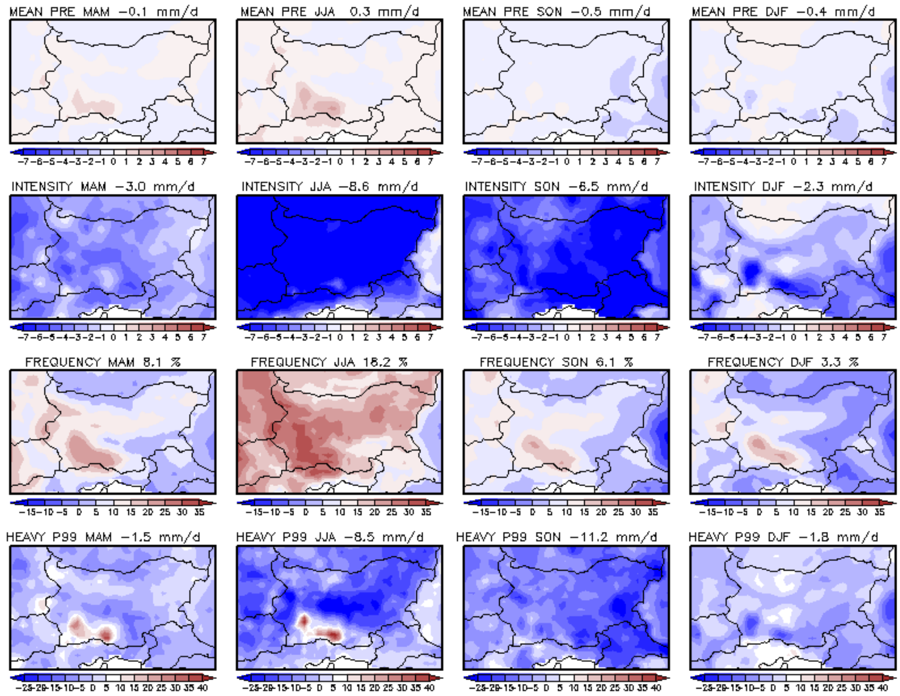

(**b**) RegCM_15 km vs. CHIRPS

Figure 5. Same as Figure 4, but between (**a**) CP_RegCM_3 km and CHIRPS; and (**b**) RegCM_15 km and CHIRPS. The domain grid size is 19.91° E–30.09° E, 39.76° N–45.32° N.

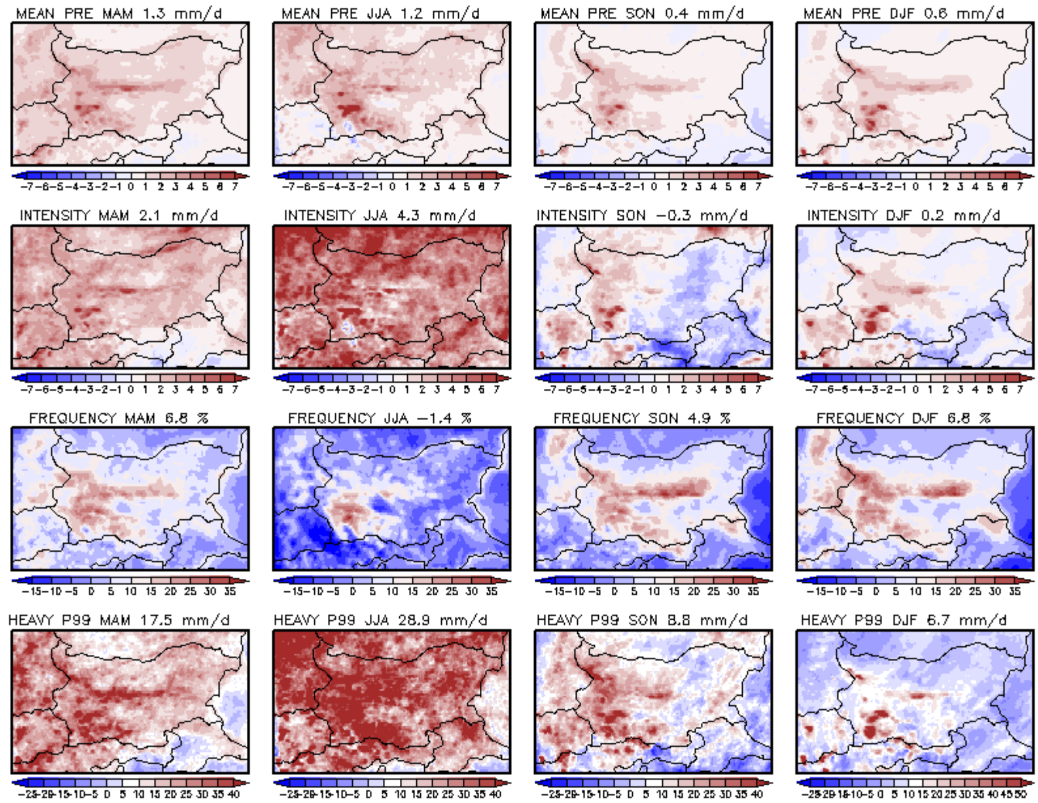

(**a**) CP_RegCM_3 km vs. MESCAN-SURFEX

Figure 6. *Cont.*

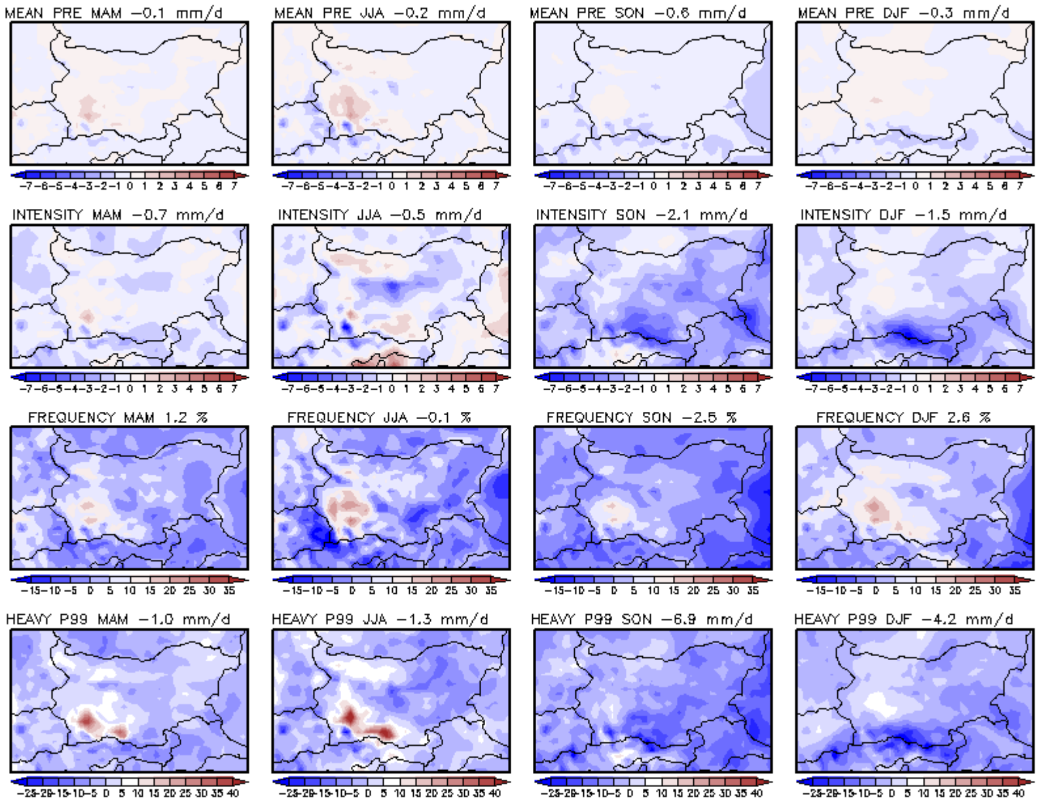

(**b**) RegCM_15 km vs. MESCAN-SURFEX

Figure 6. Same as Figure 4, but between (**a**) CP_RegCM_3 km and MESCAN; and (**b**) RegCM_15 km and MESCAN. The domain grid size is 19.91° E–30.09° E, 39.76° N–45.32° N.

Table 3. Area average mean and biases for daily precipitation metrics. The improvements in CP simulation are marked in bold.

DAILY	CHIRPS	MESCAN	E−OBS	RCM3	RCM15	RCM3−CHIRPS	RCM15−CHIRPS	RCM3−MESCAN	RCM15−MESCAN	RCM3−E−OBS	RCM15−E−OBS
MEAN PRECIPITATION mm/d											
MAM	1.9	1.9	1.5	3.2	1.8	1.3	−0.1	1.3	−0.1	1.9	0.4
JJA	1.8	2.3	1.6	3.5	2.1	1.7	0.3	1.2	−0.2	2.2	0.7
SON	2	2.1	1.8	2.5	1.5	0.5	−0.5	**0.4**	−0.6	0.8	−0.3
DJF	2	1.9	1.6	2.5	1.7	0.5	−0.4	0.6	−0.3	1.0	0.1
INTENSITY mm/d											
MAM	8.6	6.3	6	8.4	5.6	**−0.1**	−3.0	2.1	−0.7	2.6	−0.3
JJA	15.4	7.4	7.8	11.7	6.9	**−3.7**	−8.6	4.3	−0.5	4.2	−0.9
SON	12.5	8.2	7.9	8	6.1	**−4.6**	−6.5	**−0.3**	−2.1	**0.1**	−1.7
DJF	7.4	6.6	5.9	6.8	5.1	**−0.6**	−2.3	**0.2**	−1.5	0.9	−0.8
FREQUENCY %											
MAM	21.6	28.3	25.2	35.1	29.3	13.8	8.1	6.8	1.2	11.9	5.9
JJA	11.4	29.4	20.1	28	29.1	**16.9**	18.2	−1.4	−0.1	**9.8**	11.6
SON	16.2	24.7	23.1	29.6	22.3	13.6	6.1	4.9	−2.5	8.2	0.2
DJF	27.3	27.8	27.8	34.7	30.5	7.5	3.3	6.8	2.6	8.1	3.4
HEAVY PRECIPITATION P99 mm/d											
MAM	22.1	21.5	15.0	39.0	20.4	17.2	−1.5	17.5	−1.0	26.3	6.5
JJA	33.6	26.1	18.2	55.0	24.7	22.0	−8.5	28.9	−1.3	40.5	8.1
SON	32.0	27.7	20.3	36.5	20.8	**4.8**	−11.2	8.8	−6.9	17.6	1.2
DJF	20.1	22.6	14.8	29.2	18.4	9.1	−1.8	6.7	−4.2	15.0	3.6

Compared with the MESCAN dataset (Figure 6a,b and Table 3), the kilometer-scale simulation shows wet biases for mean daily precipitation (68.4% in MAM; 52.2% in JJA; 19% in SON; 31.6% in DJF) and p99 (81.4% in MAM; 110.4% in JJA; 32.4% in SON; and 29.6% in DJF) in all seasons (Figure 6a), while the coarse-scale simulation shows dry biases for mean and heavy precipitation in all seasons (Figure 6b), except in the mountains. CP_RegCM_3km shows significant overestimation of wet-day intensity and heavy precipitation (p99), especially in the summer, and wet-day frequency in SON and DJF, while RegCM_15km underestimates wet-day intensity in all seasons. Compared with the MESCAN dataset, we found improvements in CP simulation for wet-day intensity in the autumn (−3.7% vs. −26%) and winter (3% vs. 23%) and mean precipitation in the autumn (19% vs. −29%) (Table 3). The overestimation of precipitation in CP_RegCM_3km is at least partly reduced, accounting for the underestimation of precipitation in observations due to gauge under-catch and the unrepresentative height distribution of the rain gauges. The overestimation of heavy precipitation intensity has also been reported in some previous studies and may also be due to the fact that the models do not fully resolve convection [6].

The results for daily precipitation indices for all seasons are summarized in Table 3 as area-averaged means and biases. The improvements in the kilometer-scale simulation are marked in bold.

3.2. Hourly Precipitation Metrics

To analyze the spatial properties of hourly precipitation in the models, we use the following precipitation metrics (Table 2): wet-hour precipitation intensity, wet-hour frequency, and 99.9th percentiles of all (wet and dry) hourly precipitation events. A wet hour is defined as an hour with precipitation larger than or equal to 0.1 mm/hour. For assessing the precipitation metrics, we use satellite data PDIR-Now available at 0.04 degree spatial resolution (Table 1).

In the spring (Figure 7a), CP_RegCM_3km underestimates wet-hour intensity and overestimates wet-hour frequency and extreme precipitation p99.9, especially over the mountains. RegCM_15km underestimates all precipitation metrics compared with the PDIR data. In the summer (Figure 7b), CP_RegCM_3km overestimates p99.9 and wet-hour frequency and underestimates wet-hour intensity. RegCM_15km underestimates precipitation intensity and p99.9 and overestimates precipitation frequency compared with the PDIR data. The weaker RegCM_15 wet-hour intensity of precipitation and higher wet-hour frequency in the summer (Figure 7b) indicates persistent light rain, which is consistent with previous studies [6].

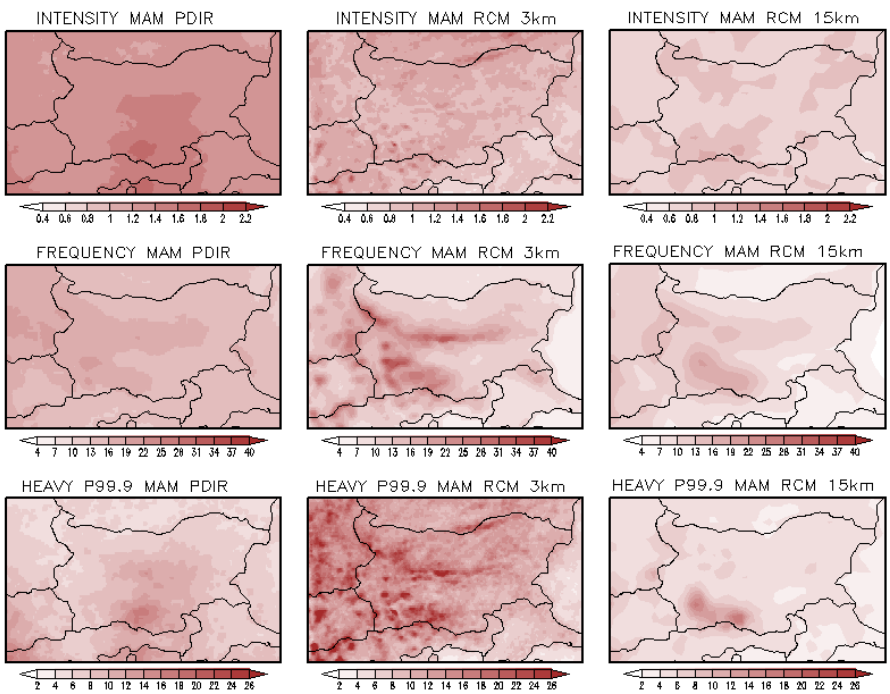

(**a**) MAM

Figure 7. *Cont.*

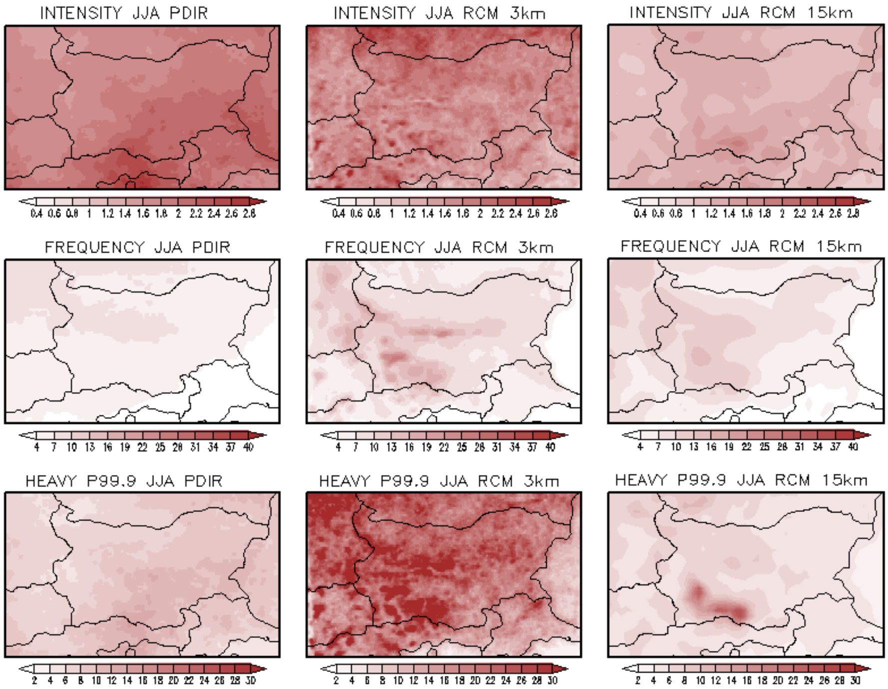

(**b**) JJA

Figure 7. Spatial distribution of analyzed indices. From top to bottom for each panel: wet-hour precipitation intensity (mm/h), wet-hour precipitation frequency (%), and heavy precipitation (mm/h), defined as the 99.9th percentile of all hourly precipitation events (wet and dry) based on observation (PDIR-Now (0.04° × 0.04°grid spacing) (first column)) and simulations (CP_RegCM_3km (second column) and RegCM_15km (third column)) for the (**a**) MAM and (**b**) JJA seasons. The domain grid size is 19.91° E–30.09° E, 39.76° N–45.32° N.

In the autumn (Figure 8a) and winter (Figure 8b), CP_RegCM3km and RegCM_15km underestimate wet-hour intensity compared with the PDIR data. CP simulation overestimates SON and DJF wet-hour frequency, especially over the mountains, and overestimates SON heavy precipitation (p99.9). RegCM_15km underestimates all precipitation metrics (compared with the PDIR data (last column for each panel)).

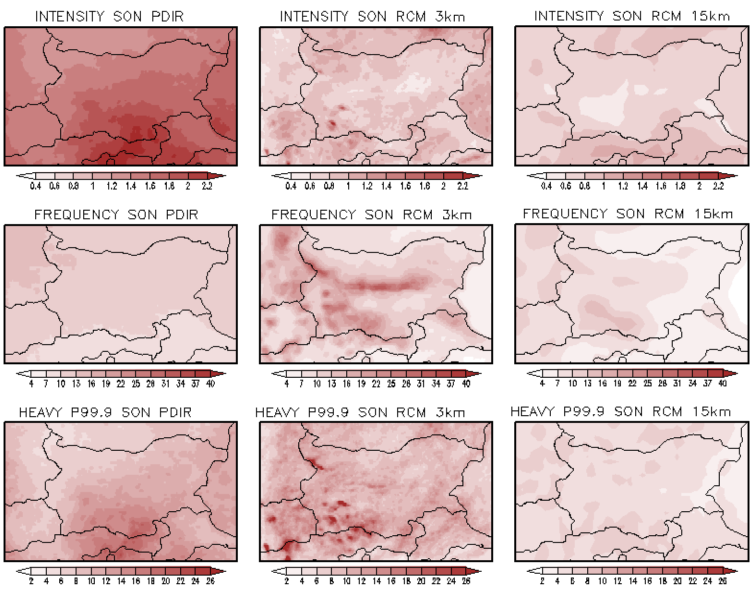

(**a**) SON

Figure 8. *Cont.*

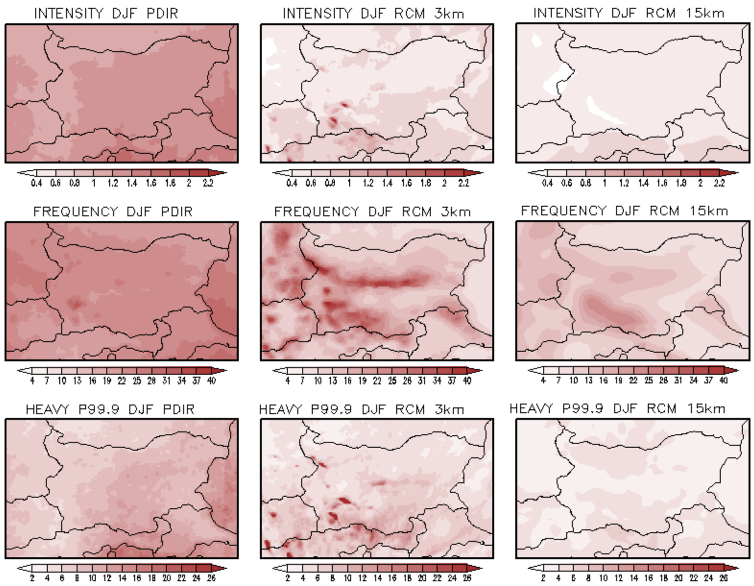

(**b**) DJF

Figure 8. Same as Figure 7, but for (**a**) SON and (**b**) DJF. The domain grid size is 19.91° E–30.09° E, 39.76° N–45.32° N.

Figure 9 shows the spatial distribution of models' mean hourly precipitation biases for intensity (mm/h), frequency (%), and heavy precipitation (p99.9) (mm/h) for Bulgaria for all seasons. CP_RegCM_3km shows dry biases for precipitation wet-hour intensity in SON and DJF, wet biases for wet-hour frequency in JJA and SON, dry biases for precipitation frequency in MAM and DJF (except in the mountains). CP simulation overestimates extreme precipitation (p99.9) in MAM and JJA and underestimates p99.9 in SON and DJF (Figure 9a). On the other hand, RegCM_15km shows dry biases for wet-hour intensity in all seasons, wet biases for precipitation wet-hour frequency in all seasons (except JJA), and dry biases for extreme precipitation (p99.9) in all seasons (except in the mountains in JJA) (Figure 9b).

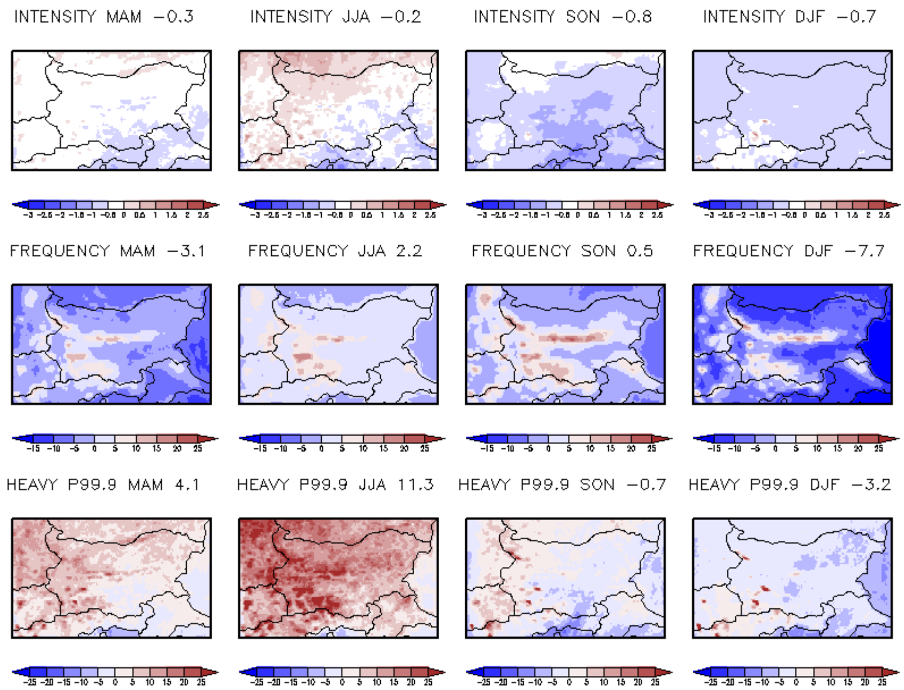

(**a**) CP_RegCM_3km vs. PDIR-Now

Figure 9. *Cont.*

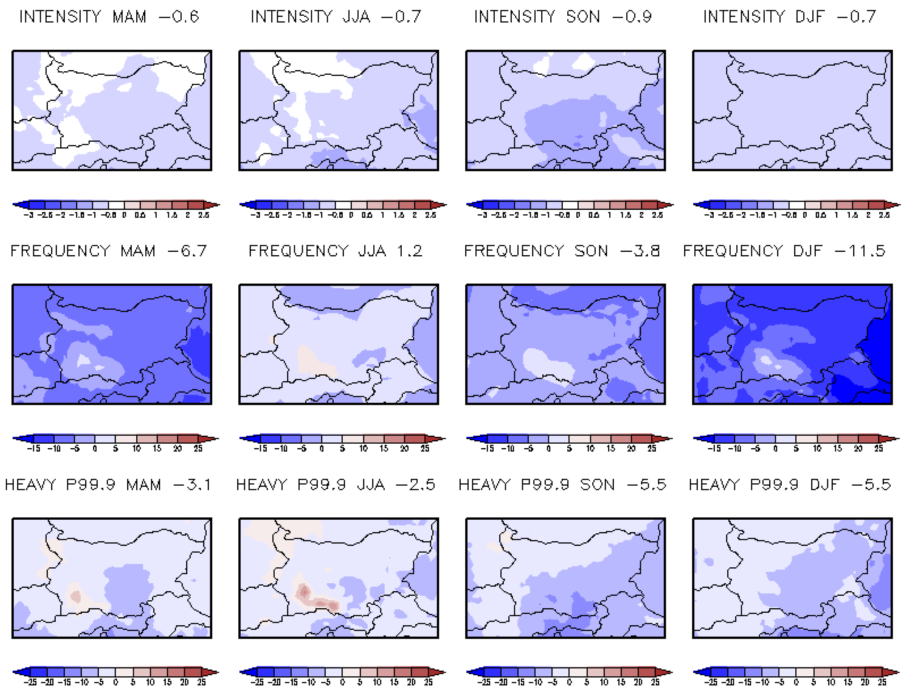

(**b**) RegCM_15 km vs. PDIR-Now

Figure 9. Spatial distribution of models' mean hourly precipitation biases for intensity (mm/h), frequency (%), and heavy precipitation (p99.9) (mm/h) for Bulgaria between (**a**) CP_RegCM_3 km and PDIR−Now; and (**b**) RegCM_15km and PDIR−Now. From left to right, the seasons are defined as spring (MAM), summer (JJA), autumn (SON), and winter (DJF) for each panel. The domain grid size is 19.91° E–30.09° E, 39.76° N–45.32° N.

Compared with the PDIR data, improvements were found in kilometer-scale simulation for wet-hour intensity in all seasons compared with coarse-resolution simulation (−23% vs. −46% in MAM; −10% vs. −37% in JJA; −47% vs. −53% in SON; −54% vs. −62% in DJF) (Table 4), for wet−hour frequency in the spring (−3.1% vs. −6.7%), autumn (0.5% vs. −3.8%), and winter (−7.7% vs. −11.5%), and for extreme precipitation (p99.9) in the autumn (−7% vs. −51%) and winter (−34% vs. −58%).

Table 4. Area average means and biases for the hourly precipitation. The improvements in CP simulation are marked in bold.

HOURLY	PDIR	RCM3	RCM15	RCM3−PDIR	RCM15−PDIR
INTENSITY mm/h					
MAM	1.3	1.0	0.8	**−0.3**	−0.6
JJA	1.9	1.7	1.2	**−0.2**	−0.7
SON	1.7	0.9	0.8	**−0.8**	−0.9
DJF	1.3	0.6	0.5	**−0.7**	−0.8
FREQUENCY %					
MAM	15.8	12.7	9.1	**−3.1**	−6.7
JJA	5.8	8.0	7.0	2.2	1.2
SON	11.4	11.9	7.6	**0.5**	−3.8
DJF	23.6	15.9	12.0	**−7.7**	−11.5
HEAVY PRECIPITATION P99.9 mm/h					
MAM	8.3	12.4	5.2	4.1	−3.1
JJA	8.6	19.9	6.1	11.3	−2.5
SON	10.8	10.0	5.3	**−0.7**	−5.5
DJF	9.5	6.3	4.0	**−3.2**	−5.5

The results for hourly precipitation metrics in MAM, JJA, SON, and DJF are summarized in Table 4 as the area-averaged means and biases. The improvements in the kilometer-scale simulation are marked in bold.

4. Discussion and Conclusions

This study presents an assessment of precipitation metrics for Bulgaria of non-hydrostatic RegCM4 [3] in climate simulation at the kilometer scale carried out as part of the Bulgarian National Science Fund project KP-06-M57/3 and is grateful for access to the EuroHPC JU Discoverer supercomputer. A convection-permitting simulation (CP_RegCM-3km) at a horizontal resolution of 3 km was conducted for the Bulgarian domain (780 km × 600 km) over a 10-year-long period (2001–2010). The assessment was performed against high-resolution observations and the driving coarse-resolution simulation (RegCM_15km) at 15 km grid spacing, forced by ERA_Interim re-analysis. We analyzed the following precipitation metrics: mean daily precipitation, precipitation wet-day/hour intensity, wet-day/hour frequency, and heavy precipitation (the 99th percentile of all daily precipitation events and the 99.9th percentile of all hourly precipitation events). The comparison among the datasets confirms the large uncertainty associated with precipitation observational data, especially when dealing with precipitation intensity and extremes.

In general, the models represent well the spatial distribution of mean precipitation at the regional and kilometer scale for the territory of Bulgaria. However, the CP_RegCM_3km model produces too much rainfall over the mountains and shows the largest biases in the summer season. At the daily scale, compared with the CHIRPS dataset, we found improvements in the kilometer-scale simulation for precipitation wet-day intensity in all seasons, in summer wet-day frequency, and in autumn extreme precipitation (p99). Compared with MESCAN, improvements were found in CP simulation for wet-day intensity in the autumn and winter seasons. Both models show a more realistic distribution of mean daily precipitation and wet-day frequency compared with MESCAN than E-OBS and CHIRPS. The observational datasets, CHIRPS and E-OBS, show similar distributions for mean precipitation, but the CHIRPS dataset shows extremely high precipitation intensities, especially in the summer and autumn. Additionally, the CHIRPS dataset underestimates precipitation wet-day frequency compared with the E-OBS data in the summer and autumn, and it overestimates heavy precipitation (p99) in the summer.

At the hourly scale, the improvement in precipitation wet-hour intensity in the CP simulation is clearer than at the daily timescale. Compared with the PDIR data, improvements were found in the kilometer-scale simulation for wet-hour intensity in all seasons compared with coarse-resolution simulation (−23% vs. −46% in MAM; −10% vs. −37% in JJA; 47% vs. −53% in SON; −54% vs. −62% in DJF) (Table 4), for wet−hour frequency in the spring (−3.1% vs. −6.7%), autumn (0.5% vs. −3.8%), and winter (−7.7% vs. −11.5%), and for extreme precipitation (p99.9) in the autumn (−7% vs. −51%) and winter (−34% vs. −58%).

CP_RegCM_3km shows an overestimation of all heavy precipitation indices over the mountains in the summer. The overestimation of precipitation in the CP simulation is at least partly reduced, considering the underestimation of precipitation in observations due to gauge under-catch and the unrepresentative height distribution of the rain gauges. The overestimation of extreme precipitation has also been reported in previous studies and may also be due to the fact that the models do not fully resolve convection [6]. Stocchi et al. [11] show that CP simulations with the RegCM4 model considerably improve precipitation extremes, intensity, and frequency biases at the hourly timescale for Italy, France, and Germany and report the largest biases for Switzerland, the Carpathians, and Greece during the summer season. They show that, at the hourly scale, the improvement in CP simulation for precipitation intensity, extreme indices, and spatial distribution is clearer than at the daily scale.

Our results—based on a newly developed non-hydrostatic RegCM4 model at a kilometer scale [3] and a set of high-resolution observational datasets—are in line with previous applications of convection-permitting regional climate models [1,2,7,10,11] and confirm the improved performance of CP models with respect to coarser resolution ones in simulating important characteristics of daily and hourly precipitation and extremes. As far as we know, convection-permitting regional climate modeling at such a high spatial resolution, specifically for the territory of Bulgaria, has not been performed before.

The availability of high-resolution observational datasets of high quality is paramount for evaluating high-resolution models, and often, such observations are not available. Uncertainties regarding in situ data are mainly linked to low station density, especially over mountain regions, and the choice of gridded techniques [35]. In the case of satellite data, the precipitation measurements can be affected by large uncertainties linked to physical limitations and measurement techniques. This is the reason why different observational datasets can have different performances of precipitation metrics and can differ significantly, especially over areas with low station availability [35]. Another aspect to consider is that many processes, which occur at the sub-kilometer scale, are still parametrized in CP models and may still require additional modifications for use at the kilometer scale. Additionally, kilometer-scale models still operate in the gray zone of turbulent motion, which means that convection is not fully resolved.

In conclusion, despite the measurement issues and persistent biases present, the convection-permitting regional climate modeling approach shows promising and encouraging results, and it is a very useful tool for future climate change studies. Our future plans are linked to climate change simulations at a convection-permitting scale and the assessment of intensity, frequency, and extreme precipitation events in the territory of Bulgaria under an RCP8.5 scenario.

Author Contributions: Conceptualization, R.V. and I.P.; methodology, R.V.; validation, R.V., I.P. and N.G.; formal analysis, R.V.; investigation, R.V.; resources, R.V., N.G. and I.P.; data curation, R.V., N.G. and I.P.; writing—original draft preparation, R.V.; visualization, N.G., I.P. and R.V.; project administration, R.V.; funding acquisition, R.V., I.P. and N.G. All authors have read and agreed to the published version of the manuscript.

Funding: This research was funded by the Bulgarian National Science Fund, grant number KP-06-M57/3.

Institutional Review Board Statement: Not applicable.

Informed Consent Statement: Not applicable.

Data Availability Statement: In this study, we used publicly archived high-resolution datasets available through the following links: E-OBS data, https://www.ecad.eu/download/ensembles/download.php, accessed on 5 May 2022; CHIRPS data, https://data.chc.ucsb.edu/products/CHIRPS-2.0/global_daily/netcdf/p05/, accessed on 2 June 2023; UERRA MESCAN-SURFEX data, https://cds.climate.copernicus.eu/cdsapp#!/dataset/reanalysis-uerra-europe-single-levels?tab=overview, accessed on 30 May 2023; and PDIR-Now data, https://chrsdata.eng.uci.edu/, accessed on 16 May 2023.

Acknowledgments: We acknowledge the funding from the Bulgarian National Science Fund, grant number KP-06-M57/3. The authors gratefully acknowledge Discoverer PetaSC and EuroHPC JU for granting access to Discoverer supercomputer resources (Sofia, Bulgaria) for this project. The authors acknowledge the Center for Hydrometeorology and Remote Sensing (CHRS) at the University of California, Irvine (UCI), for providing the PERSIANN Dynamic Infrared–Rain Rate (PERSIANN-PDIR-Now) dataset. The authors acknowledge the usage of the CHIRPS dataset from the Climate Hazards Group (https://www.chc.ucsb.edu/data, accessed on 2 June 2023); Copernicus Climate Change Service, Climate Data Store, (2019): UERRA regional reanalysis for Europe on single levels from 1961 to 2019. Copernicus Climate Change Service (C3S) Climate Data Store (CDS). https://doi.org/10.24381/cds.32b04ec5 (accessed on 30 May 2023); the E-OBS dataset from the EU-FP6 project UERRA (https://www.uerra.eu, accessed on 5 May 2022) and the Copernicus Climate Change Service, and the data providers from the ECA&D project (https://www.ecad.eu, accessed on 5 May 2022). The experiments were performed using the RegCM4.7.1 non-hydrostatic model. The RegCM4.7.1 model code is available at https://doi.org/10.5281/zenodo.4603556, accessed on 23 December 2021. We thank the Abdus Salam International Centre for Theoretical Physics (ICTP) and the Earth System Physics (ESP) group for providing free-of-charge RegCM4 software. The authors thank the anonymous referees for their helpful comments, which improved the quality of the manuscript.

Conflicts of Interest: The authors declare no conflict of interest.

References

1. Prein, A.F.; Langhans, W.; Fosser, G.; Ferrone, A.; Ban, N.; Goergen, K.; Keller, M.; Tölle, M.; Gutjahr, O.; Feser, F.; et al. A review on regional convection-permitting climate modeling: Demonstrations, prospects, and challenges. *Rev. Geophys.* **2015**, *53*, 323–361. [CrossRef] [PubMed]
2. Coppola, E.; Sobolowski, S.; Pichelli, E.; Raffaele, F.; Ahrens, B.; Anders, I.; Ban, N.; Bastin, S.; Belda, M.; Belusic, D.; et al. A first-of-its-kind multi-model convection permitting ensemble for investigating convective phenomena over Europe and the Mediterranean. *Clim. Dyn.* **2020**, *55*, 3–34. [CrossRef]
3. Coppola, E.; Stocchi, P.; Pichelli, E.; Alavez, J.A.T.; Glazer, R.; Giuliani, G.; Di Sante, F.; Nogherotto, R.; Giorgi, F. Non-Hydrostatic RegCM4 (RegCM4-NH): Model description and case studies over multiple domains. *Geosci. Model Dev.* **2021**, *14*, 7705–7723. [CrossRef]
4. Lucas-Picher, P.; Argüeso, D.; Brisson, E.; Tramblay, Y.; Berg, P.; Lemonsu, A.; Kotlarski, S.; Caillaud, C. Convection-permitting modeling with regional climate models: Latest developments and next steps. In *Wiley Interdisciplinary Reviews: Climate Change*; Wiley Online Library: Hoboken, NJ, USA, 2021; Volume 12, p. e731.
5. Déqué, M.; Rowell, D.P.; Lüthi, D.; Giorgi, F.; Christensen, J.H.; Rockel, B.; Jacob, D.; Kjellström, E.; de Castro, M.; Hurk, B.v.D. An intercomparison of regional climate simulations for Europe: Assessing uncertainties in model projections. *Clim. Change* **2007**, *81*, 53–70. [CrossRef]
6. Kendon, E.J.; Roberts, N.M.; Senior, C.A.; Roberts, M.J. Realism of Rainfall in a Very High-Resolution Regional Climate Model. *J. Clim.* **2012**, *25*, 5791–5806. [CrossRef]
7. Ban, N.; Schmidli, J.; Schär, C. Evaluation of the convection-resolving regional climate modeling approach in decade-long simulations. *J. Geophys. Res. Atmos.* **2014**, *119*, 7889–7907. [CrossRef]
8. Giorgi, F.; Coppola, E.; Solmon, F.; Mariotti, L.; Sylla, M.B.; Bi, X.; Elguindi, N.; Diro, G.T.; Nair, V.; Giuliani, G.; et al. RegCM4: Model description and preliminary tests over multiple CORDEX domains. *Clim. Res.* **2012**, *52*, 7–29. [CrossRef]
9. Hewitt, C.D.; Lowe, J.A. Toward a European Climate Prediction System. *Bull. Am. Meteorol. Soc.* **2018**, *99*, 1997–2001. [CrossRef]
10. Ban, N.; Caillaud, C.; Coppola, E.; Pichelli, E.; Sobolowski, S.; Adinolfi, M.; Ahrens, B.; Alias, A.; Anders, I.; Bastin, S.; et al. The first multi-model ensemble of regional climate simulations at kilometer-scale resolution, part I: Evaluation of precipitation. *Clim. Dyn.* **2021**, *57*, 275–302. [CrossRef]
11. Stocchi, P.; Pichelli, E.; Alavez, J.A.T.; Coppola, E.; Giuliani, G.; Giorgi, F. Non-Hydrostatic Regcm4 (Regcm4-NH): Evaluation of Precipitation Statistics at the Convection-Permitting Scale over Different Domains. *Atmosphere* **2022**, *13*, 861. [CrossRef]
12. Pichelli, E.; Coppola, E.; Sobolowski, S.; Ban, N.; Giorgi, F.; Stocchi, P.; Alias, A.; Belušić, D.; Berthou, S.; Caillaud, C.; et al. The first multi-model ensemble of regional climate simulations at kilometer-scale resolution part 2: Historical and future simulations of precipitation. *Clim. Dyn.* **2021**, *56*, 3581–3602. [CrossRef]
13. Capecchi, V.; Pasi, F.; Gozzini, B.; Brandini, C. A convection-permitting and limited-area model hindcast driven by ERA5 data: Precipitation performances in Italy. *Clim. Dyn.* **2022**, *61*, 1411–1437. [CrossRef]
14. Giordani, A.; Cerenzia, I.M.L.; Paccagnella, T.; Di Sabatino, S. SPHERA, a new convection-permitting regional reanalysis over Italy: Improving the description of heavy rainfall. *Q. J. R. Meteorol. Soc.* **2023**, *149*, 781–808. [CrossRef]
15. Adinolfi, M.; Raffa, M.; Reder, A.; Mercogliano, P. Investigation on potential and limitations of ERA5 Reanalysis downscaled on Italy by a convection-permitting model. *Clim. Dyn.* **2023**. [CrossRef]
16. Fosser, G.; Khodayar, S.; Berg, P. Benefit of convection permitting climate model simulations in the representation of convective precipitation. *Clim. Dyn.* **2015**, *44*, 45–60. [CrossRef]
17. Valcheva, R.; Spiridonov, V. Regional climate projections of heavy precipitation over the Balkan Peninsula. *Időjárás* **2023**, *127*, 77–106. [CrossRef]
18. Gadzhev, G.; Ivanov, V.; Valcheva, R.; Ganev, K.; Chervenkov, H. HPC Simulations of the Present and Projected Future Climate of the Balkan Region. In *Advances in High Performance Computing. HPC 2019. Studies in Computational Intelligence*; Dimov, I., Fidanova, S., Eds.; Springer: Cham, Switzerland, 2021; Volume 902. [CrossRef]
19. Dee, D.P.; Uppala, S.M.; Simmons, A.J.; Berrisford, P.; Poli, P.; Kobayashi, S.; Andrae, U.; Balmaseda, M.A.; Balsamo, G.; Bauer, P.; et al. The ERA-Interim reanalysis: Configuration and performance of the data assimilation system. *Q. J. R. Meteorol. Soc.* **2011**, *137*, 553–597. [CrossRef]
20. Kiehl, J.; Hack, J.; Bonan, G.; Boville, B.; Briegleb, B.; Williamson, D.; Rasch, P. *Description of the NCAR Community Climate Model (CCM3)*; NCAR Tech. Note; National Center for Atmospheric Research: Boulder, CO, USA, 1996; Volume NCAR/TN-420+STR, 159p.
21. Holtslag, A.; de Bruijn, E.; Pan, H.L. A high resolution air mass transformation model for short-range weather forecasting. *Mon. Weather Rev.* **1990**, *118*, 1561–1575. [CrossRef]
22. Pal, J.S.; Small, E.E.; Eltahir, E.A.B. Simulation of regional-scale water and energy budgets: Representation of subgrid cloud and precipitation processes within RegCM. *J. Geophys. Res. Atmos.* **2000**, *105*, 29579–29594. [CrossRef]
23. Dickinson, R.; Henderson-Sellers, A.; Kennedy, P. *Biosphere–Atmosphere Transfer Scheme (BATS) Version 1e as Coupled to the NCAR Community Climate Model*; TechRep; National Center for Atmospheric Research: Boulder, CO, USA, 1993; Volume NCAR.TN-387+STR, 80p.
24. Zeng, X.; Zhao, M.; Dickinson, R.E. Intercomparison of bulk aerodynamic algorithms for the computation of sea surface fluxes using TOGA COARE and TAO data. *J. Clim.* **1998**, *11*, 2628–2644. [CrossRef]

25. Kain, J.S.; Fritsch, J.M. A one-dimensional entraining/detraining plume model and its application in convective parameterization. *J. Atmos. Sci.* **1990**, *47*, 2784–2802. [CrossRef]
26. Kain, J.S. The Kain–Fritsch convective parameterization: An update. *J. Appl. Meteor.* **2004**, *43*, 170–181. [CrossRef]
27. Grell, G.A.; Dudhia, J.; Stauffer, D.R. *A Description of the Fifth-Generation Penn State/NCAR Mesoscale Model (MM5)*; NCAR Tech Note NCAR/TN-398 + STR; NCAR: Boulder, CO, USA, 1994.
28. Valcheva, R.; Popov, I.; Gerganov, N. A sensitivity study of the non-hydrostatic regional climate model RegCM-4.7.1 to physical parametrization schemes over the Balkan peninsula and Bulgaria, International Multidisciplinary Scientific GeoConference Surveying Geology and Mining Ecology Management. *SGEM* **2022**, *22*, 159–168. [CrossRef]
29. Schär, C.; Ban, N.; Fischer, E.M.; Rajczak, J.; Schmidli, J.; Frei, C.; Giorgi, F.; Karl, T.R.; Kendon, E.J.; Tank, A.M.G.K.; et al. Percentile indices for assessing changes in heavy precipitation events. *Clim. Change* **2016**, *137*, 201–216. [CrossRef]
30. Cornes, R.C.; Van Der Schrier, G.; van den Besselaar, E.J.M.; Jones, P.D. An Ensemble Version of the E-OBS Temperature and Precipitation Data Sets. *J. Geophys. Res. Atmos.* **2018**, *123*, 9391–9409. [CrossRef]
31. Funk, C.; Peterson, P.; Landsfeld, M.; Pedreros, D.; Verdin, J.; Shukla, S.; Husak, G.; Rowland, J.; Harrison, L.; Hoell, A.; et al. The climate hazards infrared precipitation with stations—A new environmental record for monitoring extremes. *Sci. Data* **2015**, *2*, 150066. [CrossRef] [PubMed]
32. Bazile, E.; Abida, R.; Verelle, A.; Le Moigne, P.; Szczypta, C. MESCAN-SURFEX Surface Analysis, Deliverable D2.8 of the UERRA Project. 2017. Available online: http://www.uerra.eu/publications/deliverable-reports.html (accessed on 30 May 2023).
33. Soci, C.; Bazile, E.; Besson, F.; Landelius, T. High-resolution precipitation re-analysis system for climatological purposes. *Tellus A Dyn. Meteorol. Oceanogr.* **2016**, *68*, 29879. [CrossRef]
34. Nguyen, P.; Ombadi, M.; Gorooh, V.A.; Shearer, E.J.; Sadeghi, M.; Sorooshian, S.; Hsu, K.; Bolvin, D.; Ralph, M.F. PERSIANN Dynamic Infrared-Rain Rate (PDIR-Now): A Near-real time, Quasi-Global Satellite Precipitation Dataset. *J. Hydrometeorol.* **2020**, *21*, 2893–2906. [CrossRef]
35. Prein, A.F.; Gobiet, A. Impacts of uncertainties in European gridded precipitation observations on regional climate analysis. *Int. J. Clim.* **2017**, *37*, 305–327. [CrossRef]
36. Bartsotas, N.S.; Anagnostou, E.N.; Nikolopoulos, E.I.; Kallos, G. Investigating Satellite Precipitation Uncertainty Over Complex Terrain. *J. Geophys. Res. Atmos.* **2018**, *123*, 5346–5359. [CrossRef]
37. Sarachi, S.; Hsu, K.-L.; Sorooshian, S. A Statistical Model for the Uncertainty Analysis of Satellite Precipitation Products. *J. Hydrometeorol.* **2015**, *16*, 2101–2117. [CrossRef]
38. Tian, Y.; Peters-Lidard, C.D. A global map of uncertainties in satellite-based precipitation measurements. *Geophys. Res. Lett.* **2010**, *37*. [CrossRef]

Disclaimer/Publisher's Note: The statements, opinions and data contained in all publications are solely those of the individual author(s) and contributor(s) and not of MDPI and/or the editor(s). MDPI and/or the editor(s) disclaim responsibility for any injury to people or property resulting from any ideas, methods, instructions or products referred to in the content.